accepted by ApJ, 2004 June 7

# Gamma-Ray Burst Polarization: Limits from RHESSI Measurements

C. Wigger, W. Hajdas, K. Arzner, M. Güdel, A. Zehnder

*Labor für Astrophysik, Paul Scherrer Institut, CH-5232 Villigen PSI, Switzerland*

claudia.wigger@psi.ch, wojtek.hajdas@psi.ch, arzner@astro.phys.ethz.ch, guedel@astro.phys.ethz.ch, alex.zehnder@psi.ch

## ABSTRACT

Using the RHESSI satellite as a Compton polarimeter, a recent study claimed that the prompt emission of GRB021206 was almost fully linearly polarized. This was challenged by a subsequent reanalysis. We present an novel approach, applying our method to the same data. We identify Compton scattering candidates by carefully filtering events in energy, time, and scattering geometry. Our polarization search is based on time dependent scattering rates in perpendicular directions, thus optimally excluding systematic errors. We perform simulations to obtain the instrument's polarimetric sensitivity, and these simulations include photon polarization. For GRB021206, we formally find a linear polarization degree of $\Pi_{GRB} = (41^{+57}_{-44})\%$, concluding that the data quality is insufficient to constrain the polarization degree in this case. We further applied our analysis to GRB030519B and found again a null result.

*Subject headings:* gamma rays: bursts — polarization

## 1. INTRODUCTION

One of the most outstanding problems in present-day models of the energy release in $\gamma$-ray bursts (GRB) relates to the conversion of the liberated energy into observed electromagnetic radiation. In relativistic fireball models, the pressure of the photon-lepton plasma itself leads to relativistic expansion (e.g., Piran 1999). Baryons are then accelerated through their coupling to the electrons. At a more basic level, the origin of the expanding fireball requires a definitive source of energy release that may itself be a source for mass acceleration.

Woosley & MacFadyen (1999) and MacFadyen & Woosley (1999) discuss the formation of relativistically expanding jets from hyperaccreting, stellar-mass black holes that are formed as a consequence of iron core collapse of a rotating, massive ($> 30 M_\odot$) star. Alternative models for the extraction of rotational (disk and black hole) energy and its conversion to expanding shells or jets involve magnetohydrodynamic processes, including reconnection and dynamo operation in the accretion disks (e.g, Blandford & Znajek 1977; Galeev 1979; Thompson 1996; Katz 1994, 1997; Mészáros & Rees 1997).

The most direct evidence for the presence of magnetic fields in GRB comes from their emission spectrum which is now widely interpreted in terms of synchrotron emission from relativistic electrons. Whether there is a direct connection between magnetic fields produced in the immediate environment of the GRB or the precursor star and the fields that are, at much larger distances, responsible for the observed synchrotron emission is not clear. Medvedev & Loeb (1999) argue that the required field strengths *for GRB afterglow shocks* exceed those to be expected from dragging a pre-existing progenitor field along the expanding shell, and that they also exceed field strengths that could be produced by compression of interstellar magnetic fields. A field-generating mechanism intrinsic to the shocks would thus be required. The situation is, however, less clear for the prompt GRB emission.

The recent report (Coburn & Boggs 2003) of strong linear polarization in the *prompt* $\gamma$-ray emission from GRB021206 (Hurley et al. 2002) therefore stirred some excitement. The observations were performed with the RHESSI satellite (Lin et al. 2002). From extensive modeling, the authors derived a polarization degree of $\Pi = (80 \pm 20)\%$, compatible with the assumption of maximum polarization. The emitting electrons are commonly thought to be accelerated in collisionless shocks by the Fermi mechanism to a energy distribution, $dN/dE \propto E^{-p}$, with typically $p \approx 2$. In that case, standard synchrotron theory predicts that the intrinsic polarization degree $\Pi$ is a function of $p$, namely $\Pi = (p+1)/(p+7/3)$ (Rybicki & Lightman 1979). This value therefore constitutes a maximum for a homogeneous magnetic field. For $p = 2$, one thus finds $\Pi_{\rm max} \approx 0.7$. Tangled magnetic fields with different field vectors relative to the line of sight will in general reduce $\Pi$.

The implications of these observations are far-reaching: Not only does this observation further support the synchrotron radiation model, it also seems to require nearly homogeneous magnetic fields over the source visible to the observer (a solid angle of $\approx \Gamma^{-2}$). Coburn & Boggs (2003) argue that magnetic fields dragged by the expanding shell from the surface of the exploding object are too weak to produce the prompt GRB, requiring additional turbulent shock-generated fields that, however, would produce unpolarized emission. Therefore, they suggest that the magnetic fields produced in the central engine are responsible for driving the fireball themselves. Alternatively, post-shock dynamos could generate the highly ordered

magnetic fields; but then it will have to be shown that the instabilities occur on large spatial scales (Coburn & Boggs 2003). Lyutikov et al. (2003) calculated the pulse-averaged polarization degree for a relativistically expanding shell that contains a global toroidal field. The synchrotron emission is again assumed to be from power-law distributed electrons. Their calculations predict a maximum of 60% for the polarization fraction, depending on the spectral parameters of the GRB. This view is not unequivocal. Waxman (2003) points out that a slight off-axis orientation of the relativistically expanding jet produces a strong linear polarization signal even in the presence of random magnetic fields. For further views on this, we refer to the summary in Lyutikov et al. (2003) and references cited therein.

In any case, the prospect of diagnosing magnetic field structures in the very emission region of the prompt GRB deserves upmost attention. Rutledge & Fox (2004) have reanalyzed the RHESSI data of GRB021206 and cast serious doubts on the polarization measurements reported earlier by Coburn & Boggs (2003). Rutledge & Fox (2004) conclude that the signal reported by Coburn & Boggs (2003) is either spurious or is not related to polarization, and they claim that no statistically meaningful statement can be made for the degree of linear polarization for this particular GRB.

We have reanalyzed GRB021206 and find problematic issues in both previous analyses. We find, in line with Rutledge & Fox (2004), clear evidence that much of the signal claimed by Coburn & Boggs (2003) is induced not by source polarization but by accidental coincidences of two unrelated photons arriving at the same time in two different detectors. We essentially confirm the null results of Rutledge & Fox (2004), but we present a polarization analysis that compares simultaneous scattering rates of orthogonal detector pairs and thus does not need a complicated normalization. Additionally, after implementing photon polarization in the GEANT3 software, we made extensive simulations of RHESSI's response to a fully polarized GRB. We also add one further GRB to this analysis, again finding no statistically significant evidence for non-zero polarization.

The structure of the paper is as follows: We start with a description of the RHESSI satellite and its relevant features for polarization analysis in §2. Next, we present the RHESSI data of GRB021206 in §3. In our data analysis (§4), we first select coincidence events (§4.1), before we search for a polarization signal in §4.2. Then, in §4.3, we present our simulations of a fully polarized GRB. The results of the polarization analysis of GRB021206 are presented in §5, together with the results from our simulation of a fully polarized GRB. After a quick look at GRB030519B - another candidate for polarization analysis - we compare our analysis with previous works (§6.4) and discuss in general the suitability of RHESSI as a GRB-polarimeter in §6.5.

## 2. RHESSI INSTRUMENTATION

The Reuven Ramaty High Energy Solar Spectroscopic Imager (RHESSI, Lin et al. 2002) is a NASA Small Explorer (SMEX) mission that was launched on 2002 February 5 into a low Earth orbit (600 km altitude, 38° inclination). RHESSI's primary science goal is to study solar flares in X-rays and gamma rays by using high resolution imaging spectroscopy.

The mission is equipped with a single instrument made up of two main systems: an imager and a spectrometer. The imager (Zehnder 2002) consists of a 1.5 m long tube with a set of 9 grids mounted on the front end of the tube and an identical set mounted on the rear end. The system makes use of the rotational modulation principle to obtain images of solar flares (Hurford et al. 2002). RHESSI rotates with a period of $T_{rot} \approx 4\,\mathrm{s}$ and points always towards the Sun. The spectrometer consists of nine large germanium detectors cooled to 75 K. Only weak lateral shielding was applied around the Ge-detectors. This causes RHESSI to be an all sky monitor for photons with energies above roughly 50 keV. Thus, in addition to solar observations, RHESSI is also suited for GRB observations.

### 2.1. Germanium Spectrometer

The arrangement of RHESSI's nine coaxial germanium detectors is shown in Fig. 1. They have a diameter of 7.1 cm and a height of 8.5 cm each. The cylinders are electrically segmented in a thin front segment (about 1.5 cm thick) and a thick rear segment (about 7 cm thick), for details see Smith et al. (2002). In reality the values of the front versus rear thickness may vary significantly from detector to detector. The front segments are able to detect photons from 3 keV to 2.7 MeV with a resolution (FWHM) of $\approx 1\,\mathrm{keV}$ (at 100 keV), while the rear segments are sensitive from about 20 keV to 17 MeV with a resolution of $\approx 3\,\mathrm{keV}$ (at 1 MeV). A shielding plate with holes for the detectors is placed on top of the cryostat which protects the rear segments from solar photons scattered in the cryostat materials. Similar graded Z cylinders surround the front segments and protect them from low energy background photons ($E < 100\,\mathrm{keV}$) coming from the side.

With respect to GRB observations, RHESSI's detection threshold depends on the effective shielding encountered by the incoming gamma rays. In the particular case of GRB021206, which was located at an angle of 18° with respect to the Sun's direction, the lower threshold of the rear segments was about 100 keV. This is mainly caused by absorption in the front segments and in the grid structures of the imager, absorption in the shielding plate, and absorption in the support modules located on the spacecraft equipment deck (see Fig. 2). These support modules are placed with a symmetry of 90° in order to balance the spacecraft.

The uneven mass distribution of the support modules together with the rotation of RHESSI leads to a periodic variability of the detection threshold, especially for GRBs coming in under such a small polar angle.

### 2.2. High Energy Polarimeter

RHESSI was originally designed to measure linear polarization of hard X-rays from the Sun with the help of a Be scatterer mounted in the plane of the spectrometer (McConnell et al. 2002). Solar photons pass through predefined holes in the imager tube and, after Compton scattering in the Be block, are detected in the neighboring rear segments. For Compton polarimetry of gamma rays coming from non-solar sources (and therefore missing the holes for the Be scatterer), one rather uses coincidence measurements between two detectors, one of which works as a scatterer.

The azimuthal distribution of the Compton scattered photons depends on the photon polarization: polarized photons are preferentially scattered in the direction perpendicular to the initial polarization direction. This azimuthal modulation is maximal for scattering angles of about 90°. Therefore, RHESSI's polarization sensitivity is highest for photons approaching the satellite from directions perpendicular to the detector plane, i.e. close to its rotation axis (as was the case for GRB021206). The coincidence rate of two detectors is a function of the angle between the photon polarization direction and the line through the detector centers. As this angle changes with the rotation of the satellite, the coincidence rate may exhibit a characteristic modulation pattern. Its amplitude is proportional to the polarization degree, and its period is $T_{rot}/2$. The maximum amplitude that a 100% polarized GRB would produce is an intrinsic function of the instrument and is obtained from Monte Carlo simulations.

### 2.3. Spectrometer Electronics

The detector signals are amplified by charge-sensitive preamplifiers before being sent to the Instrument Data Processing Unit (IDPU) for further analog and digital processing: amplification, digitalization, time stamping etc.. There are eighteen independent readout channels, one for each detector segment. Each detected event is defined by its detector number and segment, its arrival time and its energy channel. The event time is measured in units of binary microseconds ($1\,\mathrm{b}\mu\mathrm{s} = 2^{-20}\,\mathrm{s}$). The absolute time is known with an accuracy of a few milliseconds. The data are stored event by event in the onboard memory.

At the time of the GRBs studied here, front and rear segments of detector 2 were coupled. Its energy resolution is therefore much worse ($\approx 8\,\mathrm{keV}$ at $100\,\mathrm{keV}$). The readout of detector 2 was provided only via the front channel.

In order to save onboard memory, an automatic "decimation" procedure is applied to events in the rear segments: Only one out of $N_d$ rear events is stored for energies below a predefined threshold. This rear decimation is switched on mainly when the spacecraft is at high magnetic latitudes, where electron precipitation and cosmic ray background are high. This was the case during GRB021206 with $N_d = 4$ and energy channels below 1024 ($\approx 380\,\mathrm{keV}$).

## 3. RHESSI Data for GRB021206

We developed our own routines for the polarization search. The basic data structure we use is the event list that contains for each detected photon its arrival time, its energy and the corresponding detector segment number. The basic analysis steps are described below.

### 3.1. Light Curve and Raw Energy Spectrum

The light curve of GRB021206, extracted from the event list for all entries with energies

$$25\ \mathrm{keV} \leq\ E\ \leq 2000\ \mathrm{keV} \tag{1}$$

is shown in Fig. 3. For the polarization analysis, we selected a time interval that corresponds to exactly one rotation of RHESSI (dashed lines in Fig. 3):

$$15.08\ \mathrm{s} \leq\ t\ \leq 19.177\ \mathrm{s}\ , \tag{2}$$

where $t$ is the photon arrival time since 2002 December 6 22:49:00 UT. We find a total of about 130 800 photons in this time interval and energy band. The corresponding energy spectrum is shown in Fig. 4 (summed over all detectors and segments). The step around 380 keV is due to decimation in the rear segments. The 511 keV line originates from positron creation and annihilation in the spacecraft and the atmosphere.

The total numbers of counts in each detector segment are listed in Table 1, using the time and energy interval of Eq. (1) and Eq. (2). Detector 2 has no rear counts and a high total count rate since it is treated as an undecimated front segment. The number of counts in the other detectors varies significantly, especially in the front segments, whose thicknesses are different from detector to detector.

### 3.2. Definition of Coincidences

A photon that is Compton scattered from one detector into another one makes signals in two detectors, and thus makes two coincident entries (indices $i$ and $j$) in the event list. Naively, one would expect the real coincidences to happen within the same binary microsecond. It turns out, however, that real coincidences in the RHESSI data can have a time difference $dt = t_j - t_i$ up to 3 b$\mu$s (see below).

Compton scattering is the most important interaction of photons with Germanium at energies from 150 keV up to a few MeV. The energy $k_1$ of a Compton scattered photon is

$$k_1 = \frac{k_0}{1 + (k_0/m_e) \cdot (1 - \cos\theta)} \tag{3}$$

where $k_0$ is the initial photon energy, $m_e$ the electron mass and $\theta$ the scattering angle between in- and out-going photon. The kinetic energy $E_e$ of the recoil electron is

$$E_e = k_0 - k_1 \tag{4}$$

For a 150 keV photon that makes a Compton scattering with $\theta = 90°$ the energy of the recoil electron is $E_e \approx 35$ keV. In our observation, low energy noise dominates below about 15 keV (see Fig. 4). We therefore require for the energies $E_i$ and $E_j$ of a coincidence pair ("energy cut"):

$$\begin{aligned} 25 \text{ keV} &\leq E_k\,, \qquad k = i, j \\ 150 \text{ keV} &\leq E_i + E_j \leq 2000 \text{ keV} \end{aligned} \tag{5}$$

If we assume that the total energy of the scattered photon is measured in one of the Ge detectors, and the total energy $E_e$ of the recoil electron in the other one, we can calculate the scattering angle $\theta$ from the above equation (3), namely

$$\cos\theta = 1 - \frac{E_e}{k_1} \cdot \frac{m_e}{E_e + k_1}\,. \tag{6}$$

By taking into account the geometry of the detectors and the space in between we allow $\theta$ within $90° \pm 45°$. This rather generous angle range corresponds to $0.3 \leq 1 - \cos\theta \leq 1.7$. For each event pair (energies $E_i$ and $E_j$) we can therefore apply an additional energy cut ("kinematical cut"), namely

$$\begin{aligned} 0.3 &\leq \frac{E_i}{E_j} \cdot \frac{m_e}{E_i + E_j} \leq 1.7 \\ &\text{or} \\ 0.3 &\leq \frac{E_j}{E_i} \cdot \frac{m_e}{E_i + E_j} \leq 1.7\ . \end{aligned} \tag{7}$$

Because we do not know which detector observed the scattered photon and which one the recoil electron, we have to test both combinations.

Concerning the accepted detector pairs, we distinguish between spatially *close* and *distant* detector pairs, see Fig. 1. Among the 36 possible pairs we have 19 close and 17 distant pairs. The chance of a real Compton scattered event between distant detectors is considerably smaller than between close detectors. For pairs like e.g. detectors 2 and 6, it is essentially zero because detector 7 is located in between. Since the mean free path of a Compton scattered photon is about 1 to 2 cm, it would be stopped or scattered in detector 7. Indeed, when the analysis was performed with the distant detector pairs only, an insignificant number of Compton scattering candidates was found (see Section 5.4). The acceptance of only close detector pairs is called "close pairs cut".

In order to find the time difference $dt$ of *real* coincidences, we study the number of pairs as a function of $dt$ for *any* two events (not only two consecutive entries in the event list) fulfilling (2) and (5), and occurring in a pair of close detectors. Fig. 5 shows six plots which represent the possible combinations between the involved electronics (`F`: front segments, `R`: rear segments, and `2`: the unsegmented detector 2). `RF`, for instance, stands for pairs for which one signal occurred in a rear segment and the other in a front segment, and $dt$ is defined as the time difference between front and rear. Negative $dt$-values indicate cases where the front signal occurred earlier than the rear signal. In order to obtain positive and negative time differences in the cases of `RR` or `FF` pairs, we arbitrarily choose to subtract the time of the detector with the lower number from the time of the partner with the higher number. This does not affect our further analysis. `RR,2xDec` stands for coincidences between two rear segments, where both energies $E_i$ and $E_j$ are within the decimated range.

The structure in the $dt$-plot of the `RR,2xDec`-pairs shows a period of 4 b$\mu$s, which is due to the decimation procedure with $N_d = 4$. Decimation in the rear segment works like a clocked veto (Curtis 1999): During 1 b$\mu$s, the events in all detectors are accepted, during the next $(N_d - 1)$ b$\mu$s they are all rejected.

The real coincidences are clearly visible in Fig. 5. We find that they appear at different time differences $dt$, mainly at:

$$\begin{aligned}
&\texttt{FF} \;:\; dt = 0 \text{ b}\mu\text{s} \\
&\texttt{RR} \;:\; dt = 0 \text{ b}\mu\text{s} \\
&\texttt{RF} \;:\; dt = 1 \text{ b}\mu\text{s} \quad \text{or} \quad dt = 2 \text{ b}\mu\text{s} \\
&\texttt{F2} \;:\; dt = 1 \text{ b}\mu\text{s} \\
&\texttt{R2} \;:\; dt = 2 \text{ b}\mu\text{s} \quad \text{or} \quad dt = 3 \text{ b}\mu\text{s} \; .
\end{aligned} \tag{8}$$

These time bins are indicated in Fig. 5 by the vertical gray lines, and they are used as "*dt*-cut". Coincidences outside these time bins are accidental coincidences. We think that the different $dt$ are caused by different delays in the readout channels: The rear segment electronics is fastest, the time stamp in the front segments is on average 1.6 b$\mu$s later, and detector 2 is about 2.6 b$\mu$s later.

## 4. ANALYSIS METHOD

### 4.1. Coincidence Types

The high photon rate during GRB021206 introduces numerous accidental coincidences. Their rate can be determined from Fig. 5. We use the accidental coincidences with 12 b$\mu$s $\leq |dt| \leq$ 31 b$\mu$s (so-called "time shifted coincidences") and interpolate them around $dt = 0$ (see Fig. 5). The time differences $|dt|$ used to estimate the number of accidentals should on the one hand be higher than the longest readout time of the events, i.e., longer than a few b$\mu$s. On the other hand, it should be smaller than the shortest time scale of variability in the GRB light curve.

The total number of coincidences ($N_{tot}$) as well as the number of accidental coincidences ($N_{acc}$) can be determined for any time interval, leading to time dependent functions $N_{tot}(t_i)$ and $N_{acc}(t_i)$. The number $N_{acc}(t_i)$ is proportional to the square of the total count rate, and therefore shows a strong time variation.

Some of the real coincidences observed during the GRB are induced by various background components. We call this number $N_{BG}$. It could show a rotation angle dependent time variation and can be estimated by interpolation of the data before and after the GRB:

$$\begin{aligned} N_{BG}(t_i) &= 0.5 \cdot (N_{tot}(t_{i,1}) - N_{acc}(t_{i,1})) \\ &+ 0.5 \cdot (N_{tot}(t_{i,2}) - N_{acc}(t_{i,2})) \ , \end{aligned} \tag{9}$$

where $t_{i,1}$ denotes a time bin before and $t_{i,2}$ a time bin after the GRB, with equal rotation angle of RHESSI as at time $t_i$.

The remaining number of coincidences, namely

$$N_C(t_i) = N_{tot}(t_i) - N_{acc}(t_i) - N_{BG}(t_i) \ , \tag{10}$$

are called "Compton scattering candidates" and includes the real Compton scattering events.

A closer look at all the close detector pairs that fulfill the energy cut (5), the kinematical cut (7), and and the *dt*-cut (8) shows that many of them are part of a multiple coincidence

(3 or more detector segments firing at the same time). It often happens that a photon undergoes a forward Compton scattering in a front segment before being Compton scattered in the rear segment into a neighboring detector. In other cases, several detectors observe a signal. This is relatively more often the case before and after the GRB. Multiple coincidences can be caused by nuclear reactions, bremsstrahlung, or pair/photon cascades originating from the passage of high energy cosmic rays through the spacecraft. None of these multiple coincidences contribute to a polarization signal. We therefore do not accept them.

We identify multiple coincidences by looking at all accepted coincidences. Let $t_C$ be the time of a coincidence, more exactly, the earlier time of the two events involved. Two coincidences are members of a multiple coincidence if $|t_{C,1} - t_{C,2}| \leq 2\,\mathrm{b}\mu\mathrm{s}$. All coincidences that fulfill this condition are rejected (so-called "no-multiples cut"). However, members of multiple coincidences are also members of time shifted coincidences used to determine the number of accidental coincidences. In order to obtain the correct number of accidental coincidences, we clean the initial event list from members of multiple coincidences. We then search again for real and time shifted coincidences.

### 4.2. Polarization Analysis

In order to search for a polarization signal we first note that all close detector pairs can naturally be grouped into four scattering directions (see Fig. 1), each separated by 45°. According to a RHESSI-fixed coordinate system, we call these directions the 0° direction, the 45° direction, the 90° direction, and the 135° direction. The true pair angles, measured from detector center to detector center, vary slightly. The mean deviation from the nominal value is $\approx 3°$ with a maximum of 8.4°. This is much less then the width of scattering angles accepted by a detector pair, which is of the order 30°.

Assuming that polarized photons at a time $t_0$ were scattered preferentially in the 135° direction, then, one eighth of a satellite rotation later, they would be scattered preferentially in the 90°-direction. After another rotation by 45°, they would be scattered in the 45°-direction, and so on.

We determine the number of Compton scattering candidates for the 4 scattering directions and call them $N_{C,x}$, with $x \in \{\ 0,\ 45,\ 90,\ 135\ \}$. For a GRB with a strongly varying light curve, such as GRB021206, the $N_{C,x}(t_i)$ are strongly correlated with the light curve. Let $n_x(t_i)$ be the normalized coincidence light curves,

$$n_x(t_i) = \frac{N_{C,x}(t_i)}{\sum_i N_{C,x}(t_i)}\ , \tag{11}$$

where the sums are over the entire time interval used for polarization analysis (typically one or more full rotations, e.g. Eq. (2)). We can then define the following asymmetries:

$$\begin{aligned} A_{135-45}(t_i) &= \frac{n_{135}(t_i) - n_{45}(t_i)}{n_{135}(t_i) + n_{45}(t_i)} \\ A_{90-0}(t_i) &= \frac{n_{90}(t_i) - n_0(t_i)}{n_{90}(t_i) + n_0(t_i)} \ , \end{aligned} \tag{12}$$

For an *unpolarized* GRB, we make the plausible assumption that the $N_{C,x}(t_i)$ are approximately proportional to each other, i.e. we assume that there exists a time dependent function $f(t_i)$ and factors $B_x$ such that we can write $N_{C,x}(t_i) \approx B_x \cdot f(t_i)$. The factors $B_x$ take into account the efficiencies of the four scattering directions, while $f(t_i)$ is closely related to the light curve of the GRB. In that case, the asymmetries (12) are always zero (within statistical errors). In the case of a *polarized* GRB, an additional sinusoidal time dependence is introduced:

$$\begin{aligned} N_{C,x}(t_i) \approx B_x \cdot f(t_i) \\ \cdot(1 + \mu_p \cos(\omega t_i - \phi - \phi_x)) \ . \end{aligned} \tag{13}$$

The observation of a non-zero modulation amplitude $\mu_p$ would be an indication of a GRB polarization. Simulations show that $\mu_p$ is of order 0.2 for a 100 % polarized GRB. The expected periodicity of the modulation is $\omega = 2\pi/(T_{rot}/2)$. The absolute phase $\phi$ is unknown, and the relative phase shifts are fixed at $\phi_{135} = 0$, $\phi_{90} = \pi/2$, $\phi_{45} = \pi$, and $\phi_{90} = 3\pi/2$. From Eqs. (11)-(13), we obtain

$$\begin{aligned} A_{135-45}(t) &\approx \mu_p \cdot \cos(\omega t - \phi) \\ A_{90-0}(t) &\approx \mu_p \cdot \cos\left(\omega t - \phi - \frac{\pi}{2}\right) \ . \end{aligned} \tag{14}$$

The definition of the asymmetries $A_{135-45}(t)$ and $A_{90-0}(t)$ uses only data. By making a fit, the best values for the observable modulation amplitude $\mu_p$ and the phase $\phi$ can be determined. In order to obtain the real polarization degree of a GRB, $\mu_p$ should be compared with $\mu_{100}$ obtained from the simulation of a 100% polarized GRB, analyzed the same way.

### 4.3. Simulations

The standard RHESSI software provides energy deconvolution routines, using simulated response functions, but only for solar photons. Therefore we have rerun the simulation code, but for off-axis photons.

All essential parts of the satellite are built into a mass model using the GEANT3.21 particle tracking code (CERN 1993). The model provides an exact description of the Ge spectrometer and its adjacent elements, e.g. graded-Z shielding, detector electronics and cryo-cooler. Other components and structures that are positioned at larger distances from the Ge detectors, maintain their mass and composition while some approximations were made for their geometry (e.g. simplified shapes) and internal arrangement (e.g. using material of mean density and Z-number). The total mass of the spacecraft is 291 kg, including 131 kg of scientific payload.

Especially for photons that arrive at an angle of less than 30° with respect to the Sun's direction (as was the case for GRB021206), the mass distribution on the equipment deck affects the light curves and spectra. The most relevant components responsible for such effects are the solid state recorder at 135° above (i.e. Sun side of) the equipment deck, the cryo-cooler power converter at 315° (above the equipment deck), the IDPU at 45° (below the equipment deck), and the battery cells at 225° (below the equipment deck), see Fig. 2 (or Lin et al. (2002), Fig.10). They all weigh of the order 10 kg.

Using the mass model of the spacecraft and the spectrometer, the RHESSI response function can be generated. For this purpose the spacecraft model in the GEANT code is illuminated by a parallel flux of gamma rays with a predefined energy spectrum and direction. All primary particles, like scattered photons, as well as secondary particles, like recoil electrons, are traced. Finally, the energy deposition in each germanium detector segment is stored.

Photon polarization is not included in GEANT3. We wrote specific routines to fully include photon polarization, using the same formalism as in the GEANT4 extension packet for low energy Compton scattering (GEANT4 2003; Heitler 1954). The momentum vector of the scattered photon and its polarization direction were generated in accordance with the Klein-Nishina formula taking into account its initial polarization.

In order to analyze the simulated data with the same program as the real data, the output of the GEANT-code was prepared to look like real data. The effects of the readout electronics were simulated by delaying the front segment events by 1.6 $\mu$s and the events in detector 2 by 2.6 $\mu$s (see end of section 3.2). Next, the time was converted into integers (in units of b$\mu$s) and the energy was converted into channels. The rear segment decimation was simulated by accepting rear segment events with energy channel $< 1024$ only if $(t \bmod 4) = 0$. We also added events as cosmic induced background. In order to obtain good statistics, we simulated the GRB lasting over many rotations (typically 10 to 40). A very high photon rate per rotation would introduce a very high accidental coincidence rate.

# 5. RESULTS

## 5.1. Results from GRB021206

We start the data analysis of GRB021206 by identifying possible coincidences. Possible coincidences are event pairs that have a time difference $dt \leq 3\,\mathrm{b}\mu\mathrm{s}$, belong to the time interval given in Eq. (2), and fulfill the energy cut (5). We find 16542 such pairs, see Table 2. Using the method described in section 4.1 to determine $N_{acc}$ and $N_{BG}$, we find 1641 Compton scattering candidates. The effects of successively applying the $dt$-cut, the close pairs cut, the kinematical cut, and the no-multiples cut are listed in Table 2. The $dt$-cut and the close pairs cut affect the number of Compton scattering candidates only slightly, but are both very effective in reducing the number of accidental coincidences, as can be seen from Table 2. The kinematical cut seems less effective. However, simulations show that the modulation amplitude is about 15% higher when using the kinematical cut. The sequence of the energy cut, the $dt$-cut, the close pairs cut and the kinematical cut is interchangeable. The last line of Table 2 is obtained after applying the no-multiples cut. The no-multiples cuts is not interchangeable with the other cuts. The quite big effect of the no-multiples cut can be explained by the fact that multiple coincidences can lead to comparably many double coincidences. A triple coincidence of, e.g., detector 2, rear segment 3 and rear segment 5 can lead to three accepted coincidences. Multiple coincidences that include 4 or more detector segments will cause even more double coincidences.

The time dependent total coincidence rate $N_{tot}(t_i)$ of GRB021206 is plotted in Fig. 6 (crosses), together with the number $N_{acc}(t_i)$ of accidentals (gray filled histogram). Both $N_{tot}$ and $N_{acc}$ were determined as described in section 4.1. It can be seen that a large fraction of all coincidences during the GRB are accidentals. Before and after the GRB, we observe background coincidences. The number of accidental coincidences is very small before and after the GRB.

We note at this point that the energies of the background coincidences are on average higher than those of the GRB coincidences. We also observed that the percentage of multiple coincidences is higher among the background coincidences than among the GRB induced coincidences.

We obtain a total of $N_{tot} = 2141\,(\pm 46)$ coincidences in the time interval between the two dashed long vertical lines of Fig. 6, and $N_{acc} = 1081\,(\pm 10)$ accidental coincidences (the error is $\sqrt{1081/10}$ because the interpolation of the accidentals relies on 10 times better statistics). From the time interval before and after the GRB (indicated by the short dashed lines in Fig.

6) we determine the number of background coincidences as $N_{BG} = 290\,(\pm 12)$. Thus we find

$$\text{GRB021206:} \qquad N_C = 770 \pm 49 \tag{15}$$

Compton scattering candidates. The cited errors are purely statistical.

The time distributions of the Compton scattering candidates during the GRB ($N_{C,x}(t_i)$) are plotted in Fig. 7 for the four possible scattering directions (see section 4.2). The two directions in each plot make an angle of 90°. If, in case of a polarized burst, one curve showed a relative maximum compared to the other curve, 4 bins later ($\approx 1.0\,\mathrm{s}$) the other curve would show a relative maximum. Additionally, the two plots are related by the fact that a relative maximum in the light curve of the 135° direction (upper plot) would appear 2 bins ($\approx 0.5\,\mathrm{s}$) later in the 90° direction (lower plot). No such effect can be seen by visual inspection.

The asymmetries $A_{135-45}$ and $A_{90-0}$, defined in Eq. (12), are plotted in Fig. 8, together with the best fit of the function (14). Since the two curves are connected by a fix phase, we fit them simultaneously in order to obtain the two free parameters, namely the asymmetry amplitude $\mu_p$ and the phase $\phi$. The fit result for the modulation amplitude is

$$\text{GRB021206:} \qquad \mu_p = (8.6 \pm 9.4)\% \tag{16}$$

with a $\chi^2$ of 14.0 (28 DoF).

### 5.2. Results from GRB030519B

We have also studied GRB030519B (Lamb at al. 2003; Hurley et al. 2003) as another good candidate for polarization analysis. GRB030519B is also very strong and occurred at an angle of 165° with respect to the direction toward the Sun, i.e. it came from the antisolar side at an anlge of only 15°. There was no decimation during this observation.

With the method described in section 4, but including two full rotations from 14:04:53.80 to 14:05:02.062 UT, we obtain a total of $N_{tot} = 1471\,(\pm 38)$ coincidences, $N_{acc} = 144\,(\pm 4)$ accidental coincidences, and the number of background coincidences is $N_{BG} = 710\,(\pm 19)$, resulting in

$$\text{GRB030529B:} \qquad N_C = 617 \pm 43 \tag{17}$$

Compton scattering candidates. More than half of the coincidences originate from background. The more than three times higher value for the background coincidences (compared with GRB021206) can be explained by the two times longer GRB time interval, and by the undecimated data.

The fitted amplitude is

$$\text{GRB030529B:} \qquad \mu_p = (4.7 \pm 8.6)\% \tag{18}$$

with a $\chi^2$ of 11.7 (28 DoF).

### 5.3. Results from simulations

The initial energy spectrum is simulated between 25 keV and 5 MeV with a spectral shape that follows a simple power law: $dN/dE \propto E^{-\alpha}$, where $dN/dE$ is the number of photons per energy interval. We made simulations of fully polarized GRBs with power law indices $\alpha = 2.4$, 2.6, and 2.8 . These simulations were made with uniform time distribution, corresponding to a constant flux during the burst. Between 150 keV and 2 MeV, a power law index of $\alpha = 2.6$ gives a detected spectrum that agrees well with the one of GRB021206, see Fig. 9.

We also made a high-statistics simulation of a fully polarized GRB with $\alpha = 2.6$ taking into account the highly variable light curve of GRB021206. After applying decimation, we found $N_{C,sim} = 4203\,(\pm 82)$ Compton scattering candidates. The asymmetry plot for this simulation is shown in Fig. 10. The fitted modulation amplitude is

$$\mu_{100} = (21.0 \pm 2.7)\%. \tag{19}$$

The fit result for the phase, $\phi = (87.2 \pm 7.5)^\circ$, is in good agreement with the simulated value of 82.7°. The $\chi^2$ in the fit is 28.9 (28 DoF). The error bars have different length because of the statistical errors of the underlying light curve. A uniform time distribution gives error bars of similar length.

The fitted asymmetry modulations $\mu_{100}$ are plotted as a function of $\alpha$ in Fig. 11. At $\alpha = 2.6$ we have two simulations with uniform time distribution (called 'A' and 'B') and one taking into account the light curve variation (called 'ltc'). The values obtained by including decimation are marked with diamonds, undecimated results are marked by triangles. The mean value of the uniform simulations, with decimation, is $\mu_{100} = (22.9 \pm 2.7)\%$, in good agreement with Eq. (19).

We conclude from Fig. 11: (i) Within statistical errors, decimation does not affect the modulation amplitude $\mu_{100}$ , (ii) $\mu_{100}$ does not depend significantly on the power law index $\alpha$ in the range 2.4 – 2.8, (iii) $\mu_{100}$ does not depend on the light curve variation. This can be understood because each time bin can be thought of as an independent experiment. Whether they are simulated with more or less statistics should not bias the result.

The simulations also show that less than half of the so-called Compton scattering candidates are due to the process we want to analyze: an incoming photon undergoes its first interaction within a RHESSI detector and is then Compton scattered into a second detector, without additional intervening interaction. Some photons undergo a first interaction before they reach a germanium detector (of the order 20%). Other photons are scattered twice in the first detector before being detected in a second detector (of the order 40%).

We also made simulations with unpolarized photons and a power law index $\alpha = 2.6$. We obtain (decimation is applied) $\mu_{unpol} = (5.3 \pm 5.4)\,\%$ for uniform time distribution and $\mu_{unpol} = (2.5 \pm 2.7)\,\%$ for a simulation taking into account the light curve of GRB021206. Both fits agree with $\mu_{unpol} = 0$ within statistics.

Simulations of GRB030519B gave comparable values for the modulation amplitude $\mu_{100}$ as the simulations of GRB021206.

The fraction of accidental coincidences was chosen to be small in these simulations. A high fraction of accidental coincidences would increase the statistical errors.

### 5.4. Distant detector pairs

As a test, we determined the number of Compton scattering candidates as described in section 4.1, for the 17 distant detector pairs instead of the close detector pairs. From *simulations* we obtain a ratio

$$N_{C,dist}/N_{C,close} \approx (11 \pm 1)\% \; . \tag{20}$$

With the data of *GRB021206*, we obtain for the distant detector pairs: $N_{tot} = 1007\,(\pm 32)$, $N_{acc} = 839\,(\pm 9)$, $N_{BG} = 154\,(\pm 9)$, and therefore $N_{C,dist,obs} = 16\,(\pm 34)$. Combining Eq. (15) with Eq. (20), we would expect $N_{C,dist,ex} = 85\,(\pm 9)$. This is slightly higher than the observed number.

With the data of *GRB030519B*, we obtain for the distant detector pairs: $N_{tot} = 566\,(\pm 24)$, $N_{acc} = 147\,(\pm 4)$, $N_{BG} = 345\,(\pm 13)$, and therefore $N_{C,dist,obs} = 74\,(\pm 28)$. Combining Eq. (17) with Eq. (20), we would expect $N_{C,dist,ex} = 68\,(\pm 8)$. This is in excellent agreement with the observed number.

The results show that the distant pairs do not contribute significantly to the number of Compton scattering candidates.

# 6. DISCUSSION

## 6.1. Summary of our method and results

We select and identify coincidences according to the parameters given in Sect. 3.2 and 4.1. The efficiencies of the cuts used are listed in Table 2. These narrow cuts lead to a comparably small error for the number of Compton scattering candidates (see section 6.4).

By comparing scattered events in two directions that make a relative angle of 90°, we eliminate most systematic effects induced by the strongly varying light curve. The asymmetry plot we present in Fig. 8 is entirely based on observational data; simulations are only necessary to find the possible degree of polarization.

When processing simulated data of a fully polarized GRB with our method, we find a modulation $\mu_{100}$ of the order 20 to 25% (see Fig. 11). The observed value $\mu_p$ has to be compared with the simulated value $\mu_{100}$ to obtain the polarization degree $\Pi_{GRB}$ of a GRB:

$$\mu_p = \Pi_{GRB} \cdot \mu_{100} \ . \tag{21}$$

From theoretical considerations (see Sect. 1), a maximum polarization of $\Pi_{max} \approx 0.7$ is expected. Thus, the maximum observable modulation amplitude $\mu_{max}$ is of the order 15%.

The data of both GRBs presented, namely GRB021206 and GRB030529B, agree with zero polarization (see Eq. (16) and Eq. (18)). But given the large error bars (of the order 9% for both GRBs), the maximum modulation of about 15% cannot be excluded.

The formula (21) can be written in the form $\Pi_{GRB} = \mu_p/\mu_{100}$. In the case of GRB021206 we obtain a mean value of $\Pi_{GRB} = 41\%$ for the polarization degree (using Eq. (16) and Eq. (19)). However, proper error propagation is complicated in this case. A simple estimate can be obtained by using the $1\sigma$ limits of $\mu_p$ and $\mu_{100}$: $\Pi_{GRB,min} = (8.6-9.6)/(21.0+2.7) = -3\%$ and $\Pi_{GRB,max} = (8.6 + 9.6)/(21.0 - 2.7) = 98\%$. Therefore, the result of the polarization analysis can be summarized as

$$\Pi_{\mathrm{GRB021206}} = (41^{+57}_{-44})\% \ . \tag{22}$$

## 6.2. Discussion of our method

The way we treat multiple coincidences and how we estimate the number of accidental coincidences is not fully consistent. If the photon flux is so high that the chance for triple accidental coincidences is not negligible, our method underestimates the number of Compton scattering candidates systematically. When we determine $N_{tot}$ we do not accept any triple

coincidences – including triple *accidental* coincidences –, but afterwards we again subtract the contribution from triple accidental coincidences, thus obtaining a number $N_C$ that is too low. This underestimate is smaller, the narrower the cuts for accepting coincidences. That is the reason why we apply the no-multiples cut as last cut.

In the case of GRB021206, most of the triple coincidences are physical. But some triple coincidences are purely accidental, and a comparable number of triple coincidences are mixed, i.e. a real coincidence is accidentally accompanied by an event in a third detector. We estimate that the real number of Compton scattering candidates would be of the order 50 coincidences higher than the number given in Eq. (15). An effect of the same order is expected for the distant detector pairs. The numbers cited in Sect. 5.4 for GRB021206 show that the observed number ($N_{C,dist,obs}$) of Compton scattering candidates for the distant pairs is ≈70 coincidences less than the expected number ($N_{C,dist,ex}$). This discrepancy is indeed of the order 50. To determine this number exactly is beyond the scope of this work, especially since it would only slightly affect the result of the polarization analysis and does not affect the conclusion. The estimate given above is fully sufficient for our purposes.

In the case of GRB030519B, the chance for triple accidental coincidences is very small. The number given in Eq. (17) is therefore correct. This is further confirmed by the numbers cited in Sect. 5.4, where $N_{C,dist,obs}$ and $N_{C,dist,ex}$ agree very well for GRB030519B.

Another point to discuss is the normalization we use in Eq. (11), and the assumption that the efficiencies of the four scattering directions are proportional to each other. If statistics were so good, that this approximations could not be used, the $\chi^2$ of the fit of the asymmetry plot would be too high. But even with the high-statistics Monte Carlo simulations we have performed, our fits of the asymmetry plot gave acceptable results. Another advantage of our Eqs. (11) and (12) is that the so defined asymmetry does only depend on data and thus cannot suffer from systematic errors of the simulations. We conclude that our approximations are good enough within the accuracy necessary for this work.

### 6.3. Systematic effects

We note that the light curve of GRB021206 has two maxima around 22:49:15 UT and around 22:49:17 UT. They are separated by roughly half a rotation, i.e. by the period that a possible polarization signal would have. Effects that are related to the count rate can therefore possibly be mistaken for a polarization signal.

The accidental coincidences on the one hand, are proportional to the square of the total GRB light curve: $N_{acc}(t) \propto N_0(t)^2$. If accidental coincidences are mistaken for GRB induced

real coincidences and normalized with the light curve, an effect $\propto N_0(t)$ would be observed.

Background coincidences on the other hand, are constant with time (at least approximately). If background coincidences are mistaken for GRB induced real coincidences and normalized with the light curve, this would result in an effect $\propto 1/N_0(t)$. We observed for example that when we did not subtract the background coincidences, the coincidences from distant detectors did not cancel out but showed a significant modulation.

Since we identify the Compton scattering candidates carefully, our analysis should not suffer from these effects. By comparing simultaneous scattering rates of perpendicular directions, we further minimize systematic effects related to the light curve.

### 6.4. Comparison with previous works

In Table 3 we compare our number of accepted coincidences with the results presented by Coburn & Boggs (2003) (hereafter CB) and Rutledge & Fox (2004) (hereafter RF). We would like to emphasize that the total number of coincidences ($N_{tot}$) depends *strongly* on the cuts used. The number of Compton scattering candidates ($N_C$) is less dependent on the cuts used. Its error $\sigma_{N_C}$, however, depends again on $N_{tot}$, namely $\sigma_{N_C} > \sqrt{N_{tot}}$, see Eq. (10).

We cannot confirm the high number of Compton scattering candidates found by CB, our value being more than a factor 10 lower. On the other hand, we confirm the result presented by RF, although our error is 3 times smaller.

#### *6.4.1. Comparison with CB*

We can obtain a high number of coincidences ($N_{tot}$) by widening the acceptance cuts, see first line of Table 2. But by widening the cuts we accept much more accidentals, but only a few more Compton scattering candidates. However, we cannot reproduce CB's high number $N_{tot}$ and, at the same time, their relatively small $N_{acc}/N_{tot}$-ratio.

The cuts used in CB are not described by the authors. A few details became very recently available in Boggs & Coburn (2004). In Table 3 we use the following cuts in order to reproduce CB's result: (i) time interval $14.75\,\mathrm{s} \leq t \leq 19.75\,\mathrm{s}$, (ii) as energy cut: $30\,\mathrm{keV} \leq E_k$ and $150\,\mathrm{keV} \leq E_i + E_j \leq 2000\,\mathrm{keV}$, (iii) as $dt$-cut: $|dt| \leq 3\,\mathrm{b}\mu\mathrm{s}$, (iv) no-multiples cut; the kinematical cut is not applied and all detector pairs are accepted. Our slightly higher $N_{tot}$ is probably due to a different treatment of multiple coincidences.

In order to extract the polarization signal, CB rely strongly on the simulation of a

non-polarized GRB. As a simple test of how well simulations and data agree, we can use the ratio of Compton scattering candidates to the total 0.15-2.0 MeV light curve events: $r_C = N_C/N_{0.15-2.0}$. Since $N_C$ depends on the cuts used, $r_C$ does as well. We use simulations with a low fraction of accidental coincidences in order to minimize systematic effects. Such simulations give values around $r_{C,sim} \approx 1.33\%$, depending slightly on the power law index $\alpha$, namely $dr_C/d\alpha \approx -0.35\%$. Our data analysis gives $r_{C,dat} \approx 1.2\%$, a value slightly smaller than from simulations. The likely reason is described in Sect. 6.2. If the chance of triple accidental coincidences is not negligible, as in the case of GRB021206, $N_C$ is underestimated, and therefore $r_{C,dat}$ as well. We conclude that $r_{C,dat}$ and $r_{C,sim}$ agree reasonably well using our method and simulations. If we use similar cuts to CB (see last paragraph), we obtain $r_{C,sim} \approx 1.9\%$. From Fig. 1 of CB we can estimate the total number of GRB photons in the 150 to 2000 keV band to be $N_{0.15-2.0} \approx 71\,000$ (in agreement with the number obtained from the event list). CB obtain $N_C = 9840$ Compton scattering candidates, resulting in $r_{C,CB} \approx 14\%$, i.e. in a value 7 times higher than expected from simulations. This could be another indication that CB's number of Compton scattering candidates is too high.

If CB's high number of Compton scattering candidates was partly due to accidental coincidences, the effect discussed in Sect. 6.3 were possibly responsible for the polarization signal found by CB.

CB's value for the modulation factor, $\mu_{100} = (19 \pm 4)\%$, which they obtained from simulations and analytical estimates, agrees very well with our value, if we omit the kinematical cut (7). In that case, we obtain $\mu_{100} = 18.5\%$ with a statistical error of $\pm 2.5\%$.

### *6.4.2. Comparison with RF*

The main differences between our and RF's analysis in determining the number of Compton scattering candidates are the following:

1. Instead of the *dt*-cut (8), RF mention to use $\Delta T \leq 5$ b$\mu$s. The quite high rate at $\Delta T = 4$ b$\mu$s in Fig. 2 of RF is interpreted by them as probably due to real coincidences, whereas it is caused by the decimation procedure (see Fig. 5).
   Our very narrow *dt*-cut is one of the main reason for our much smaller $N_{tot}$ and $N_{acc}$.

2. Instead of accepting only close detector pairs RF accept also distant pairs. Accepting distant detector pairs introduces mainly background noise (see section 5.4).

3. We determine the number of accidental coincidences from a time shifted coincidence window. This has the advantage of being independent of the high variability of the

GRB light curve. Different efficiencies of the detectors and effects due to the decimation procedure are also taken into account. By making the time window for the time shifted coincidences wide, we obtain a relatively small statistical error in $N_{acc}$.

4. Instead of our energy cut (5), RF use 150 keV $\leq E_k \leq$ 2000 keV. This narrower energy cut eliminates real coincidences.

5. RF replace front/rear coincidences within the same detector by a single event at the earlier time stamp. Photons that made a first interaction in the front segment before being Compton scattered in the rear segment into another detector mostly lost their polarization information in the first interaction. Such events do not contribute to the polarization signal.

6. RF use the same 5 s long time interval as CB, whereas we use 4.09 s (= one full rotation).

We also tried to reproduce RF (see Table 3) by using the following cuts in our analysis: (i) time interval 14.75 s $\leq t \leq$ 19.75 s, (ii) as energy cut: 150 keV $\leq E_i \leq$ 2000 keV, (iii) as $dt$-cut: $|dt| \leq 3\,\mathrm{b}\mu$s, (iv) no-multiples cut; all detector pairs are accepted and no kinematical cut is applied. Since RF used $|dt| \leq 4\,\mathrm{b}\mu$s as $dt$-cut (presumably, the meaning of RF's $\Delta T$ is not entirely clear) – a cut not easily feasible with our program, that takes into account the repeating 4 b$\mu$s-structure caused by decimation – we added $2/7 \cdot N_{acc}$ to $N_{tot}$ and $N_{acc}$ in order to estimate the effect of the wider $dt$-cut. RF's slightly higher value for $N_{tot}$ than our reproduction can be explained by point 5 above.

RF's polarization analysis is not clear to us. Their basic Eq. (4) is valid for Compton scattering coincidences. However, it is used for all coincidences, including about 80% accidentals, for which an expression like $N_{i,j}(t) = c \cdot N_i(t) \cdot N_j(t)$ would be more correct. We further do not understand how to get from RF's equation (7) to equation (9).

Concerning RF's Section 7, we agree with RF that the uncertainty in CB's simulation of an unpolarized GRB is not discussed in CB. But, in our view, the uncertainty in the simulation of an unpolarized GRB and the uncertainty in the simulations of $\mu_{100}$ are not as closely related as RF claim.

A further evidence that the number of accidental coincidences is much higher than presented in CB comes from the analysis of RF. RF attempted to reproduce CB although they had to estimate CB's cuts. In Fig. 7b of RF, they reproduced the "angular light curve" of CB by using a narrower energy cut than CB, but accepting $\Delta T \leq 8\mathrm{b}\mu$s. This clearly increases only the number of accidental coincidences. /bin/sh: This: command not found

The fact that RF were able to reproduce CB's angular light curve by using very different cuts can be understood, if both sets of cuts, CB's and RF's, mostly accept accidental

coincidences (R.E. Rutledge, private communication).

### 6.5. Properties of a GRB that can be searched for polarization with RHESSI

A search for GRB polarization using RHESSI data is feasible only for very strong GRBs. A fully polarized GRB would yield a modulation amplitude $\mu_{100} \approx 0.21$. In order to distinguish between *no* polarization and *full* polarization, the error $\sigma_{\mu_p}$ of the fitted modulation amplitude should be around 0.05 or smaller.

For both GRBs presented in this article we find $\sigma_{\mu_p} \approx 0.09$ (see Eqs. (16) and (18)). At first sight, it may seem surprising that both errors are similar, even though the 25-100 keV fluence of GRB021206 as measured by Ulysses was more than 5 times higher than for GRB030519B (see Hurley et al. (2002) and Hurley et al. (2003)). The main reason is the decimation of the RHESSI data. If decimation had not been active during GRB021206, RHESSI would have observed about 2.8 times more Compton scattering candidates, about 2.8 times more accidental coincidences, and about 2.2 times more background coincidences. Thus, the error $\sigma_{\mu_p}$ would be about a factor $\sqrt{2.8}$ smaller, i.e. $\sigma_{\mu_p} \approx 0.06$. This would be just above the limit to distinguish between *no* polarization and *full* polarization. Another reason for the similar $\sigma_{\mu_p}$ is the better $N_C/(N_{acc} + N_{BG})$ ratio in the case of GRB030519B, namely 0.72 compared to 0.56 for GRB021206. The error $\sigma_{N_C}$, and therefore the error $\sigma_{\mu_p}$, depends on the total number of coincidences: $\sigma_{N_C} > \sqrt{N_{tot}}$, see Eq. (10). In the case of GRB021206, $N_{tot}$ is dominated by accidental coincidences, while for GRB030519B $N_{tot}$ is dominated by background coincidences. The optimal case, however, would be if $N_{tot}$ were dominated by Compton scattering candidates.

A GRB suitable for polarization analysis with RHESSI should have a fluence comparable to GRB021206 and the data should not be decimated. Furthermore, it should last about 10 s in order to be neither dominated by accidental coincidences nor by background coincidences. For such a GRB, a polarization degree of 100% would be distinguishable from zero polarization at a confidence level of several standard deviations. Since GRB021206 was one of the strongest GRBs ever observed, the probability for such a GRB to occur is small, given that it should also come from a direction close to RHESSI's rotation axis.

## 7. CONCLUSIONS

The possibility that prompt GRB emission is strongly linearly polarized at $\gamma$-ray energies deserves attention with the advent of detectors that can potentially measure such

polarization. Polarization carries fundamental information on the orientation of magnetic fields in the source and eventually helps confine the magnetic field generation mechanism. Its detection is difficult due to various interactions in presently available detector systems. The RHESSI satellite can in principle be used as a polarimeter by using the direction dependence of Compton scattering in conjunction with the rotation of the satellite. The effects are subtle, however, and require accurate knowledge of the mass distribution of the satellite and the detector geometry. The methods essentially analyze Compton scattered GRB photons that induce coincidences in detector pairs. A principal difficulty is the separation of such events from accidental and background coincidences in the same detector pairs.

Two previous publications (Coburn & Boggs 2003; Rutledge & Fox 2004) have addressed this problem, arriving at essentially opposite conclusions for the same observed GRB. Whereas Coburn & Boggs (2003) claim to detect maximum polarization ($\Pi = 80 \pm 20\%$), Rutledge & Fox (2004) challenge this result and find no significant constraint for the polarization degree.

We have revisited the problem of GRB polarization measurements with the RHESSI satellite. Our basic test case is GRB021206 used by Coburn & Boggs (2003) and Rutledge & Fox (2004) for their respective analyses. By applying well justified selection criteria for coincidences in energy, time, and scattering angle, we found $N_C = 770 \pm 49$ Compton scattering candidates. By plotting these 770 events as "coincidence light curves" for the four different scattering directions, we could define an asymmetry and search for a possible polarization signal. We compare the result of our polarization analysis with simulations of a 100% polarized GRB. We cannot reject the null hypothesis that the burst is unpolarized, but neither can we significantly detect any non-zero polarization. The maximum possible synchrotron polarization degree would, for the measured spectral index of the burst, be of order 70%, fully compatible with the data. We conclude that *no statement on $\gamma$-ray polarization can be made for GRB021206.*

Our result contradicts the statements of Coburn & Boggs (2003), who find more than 9000 Compton scattering candidates ($N_C$) and claim to see a polarization signal at the $5.7\sigma$ level. The main problem in their analysis is the number of accidental coincidences ($N_{acc}$) that is, in our view, not determined correctly. Coburn & Boggs (2003) obtain their signal by comparing a measured "angular light curve" with simulations of an unpolarised GRB. If they do not use a correct $N_{acc}/N_C$-ratio in their simulation, then the presented simulated data points cannot be trusted.

Our result agrees in many aspects with the reanalysis presented by Rutledge & Fox (2004). By making a more sophisticated coincidence selection, we obtain much smaller errors, however. A few points of caution in the polarization analysis of Rutledge & Fox

(2004) have been mentioned in our presentation.

We also analyzed the strong GRB030519B but found fewer Compton scattering candidates than for GRB021206 and, again, no statement about the polarization degree of GRB030519B can be made.

We therefore conclude that RHESSI has not yet measured the degree of polarization of any observed GRB. Implications on magnetic field orientation based on RHESSI results are therefore premature, and the physics of magnetic field generation and structure in the $\gamma$-ray source of GRB must rely on alternative information for the time being. On the other hand, our analysis suggests that at least in principle, RHESSI does offer the capability of measuring polarization. A GRB with comparable fluence as GRB021206, but lasting $\approx 10\,\mathrm{s}$, would be required to significantly distinguish maximum polarization of a GRB from zero polarization. In addition, a GRB suitable for polarization analysis should come from a direction close to RHESSI's rotation axis.

We thank O. Wigger, A. Mchedlishvili and E. Kirk for many helpful discussions and encouragement. We also thank our referee, D.M. Smith (SCIPP, University of California, Santa Cruz), for careful reading of our manuscript and his constructive comments.

## REFERENCES

Blandford, R. D., & Znajek, R. L. 1977, MNRAS, 179, 433

Boggs, S.E., & Coburn, W., 2004, X-Ray Polarimetry Workshop, held at SLAC, Stanford, California, 9-11 February. Electronic versions of papers available under: `http://-heasarc.gsfc.nasa.gov/docs/heasarc/polar/polar.html`

CERN program Library Office, 1993, GEANT – Detector Description and Simulation Tool (CERN Geneva, Switzerland)

Coburn, W., & Boggs, S.E., 2003, Nature 423: 415

Curtis, D. W. 1999, `ftp://apollo.ssl.berkeley.edu/pub/hessi/instrument/-documents/HSI_IDPU_020A.pdf`

Galeev, A. A., Rosner, R., & Vaiana, G. S. 1979, ApJ, 229, 318

GEANT4, `http://wwwasd.web.cern.ch/wwwasd/geant4/geant4.html`

Heitler, W. 1954, The Quantum Theory of Radiation (Oxford Clarendon Press)

Hurford,G.J. et al. 2002, Solar Physics **210:** 61

Hurley, K. et al. 2002, GRB Circular Network 1727, 1728, and 2281

Hurley, K. et al. 2003, GRB Circular Network 2237

Katz, J. 1994, ApJ, 422, 248

Katz, J. 1997, ApJ, 490, 633

Lamb, D. et al. 2003, GRB Circular Network 2235 and 2238

Lin, R.P. et al. 2002, Solar Physics **210:** 3

Lyutikov, M., Pariev, V.I., & Blandford, R.D. 2003, ApJ, 597, 998

MacFadyen, A. I., & Woosley, S. E. 1999, ApJ, 524 ,262

McConnell,M.L. et al. 2002, Solar Physics **210:** 125

Medvedev, M. K., & Loeb, A. 1999, ApJ, 526, 697

Mészáros, P., & Rees, M. J. 1997, ApJ, 482, L29

Piran, T. 1999, Phys. Rep., 314, 575

Rutledge, R.E., & Fox, D.B., 2004, MNRAS, Vol. 350, p. 1288

Rybicki, G. B., & Lightman, A. P. 1979, Radiative Processes in Astrophysics (New York: JWS)

Smith,D.M., et al. 2002, Solar Physics **210:** 33

Thompson D. J. 1996, in Gamma-Ray Bursts: 3rd Huntsville Symposium, AIP Conf. Proc 384, eds. C. Kouveliotou, M. Briggs, G. Fishman (New York: AIP)

Waxman, E. 2003, Nature, 423, 388

Woosley, S. E., & MacFadyen, A. I. 1999, A&AS, 138, 499

Zehnder, A., et al. 2002, SPIE Proc. 4853, Waikoloa, Hawaii

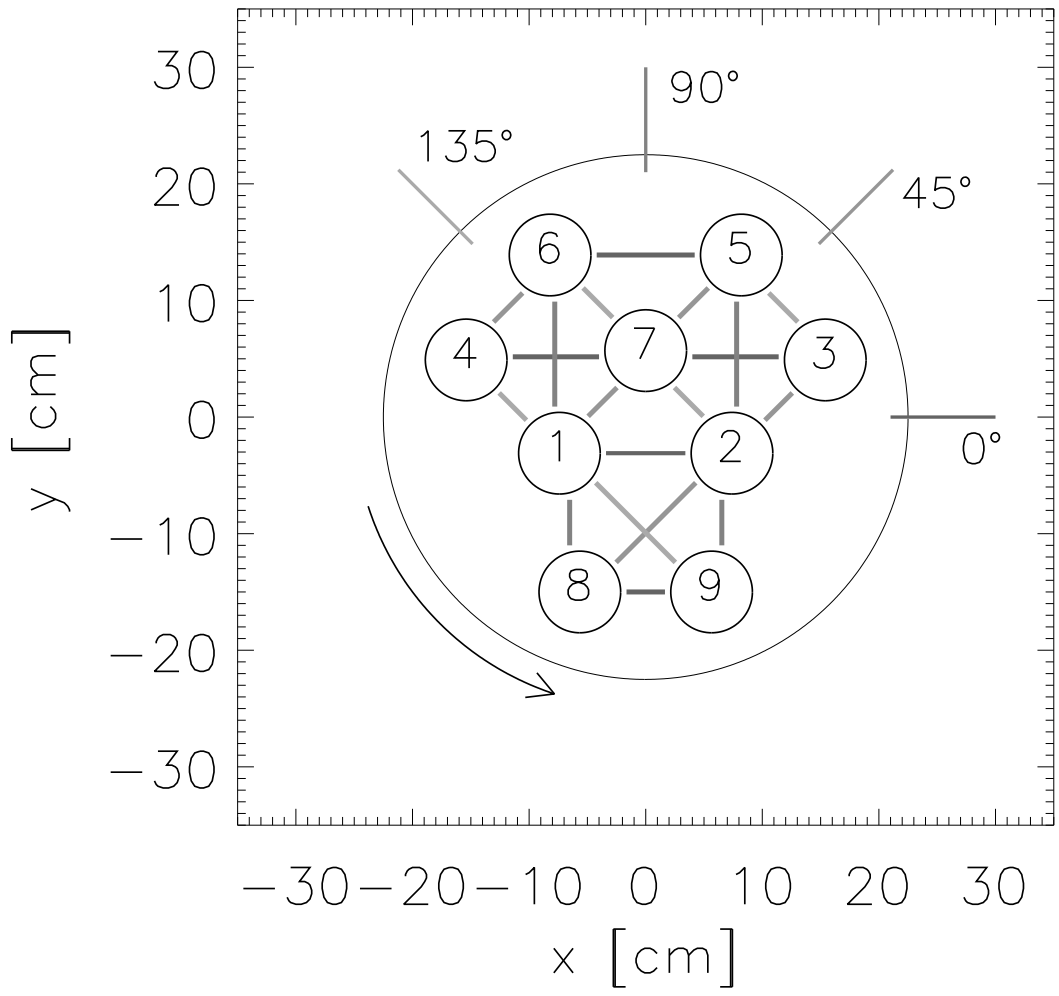


Fig. 1.— Arrangement of RHESSI's 9 germanium detectors. RHESSI spins around the axis perpendicular to the detector plane at 15 rpm. The 19 "close" detector pairs a marked by bars. They can be grouped into four possible scattering directions.

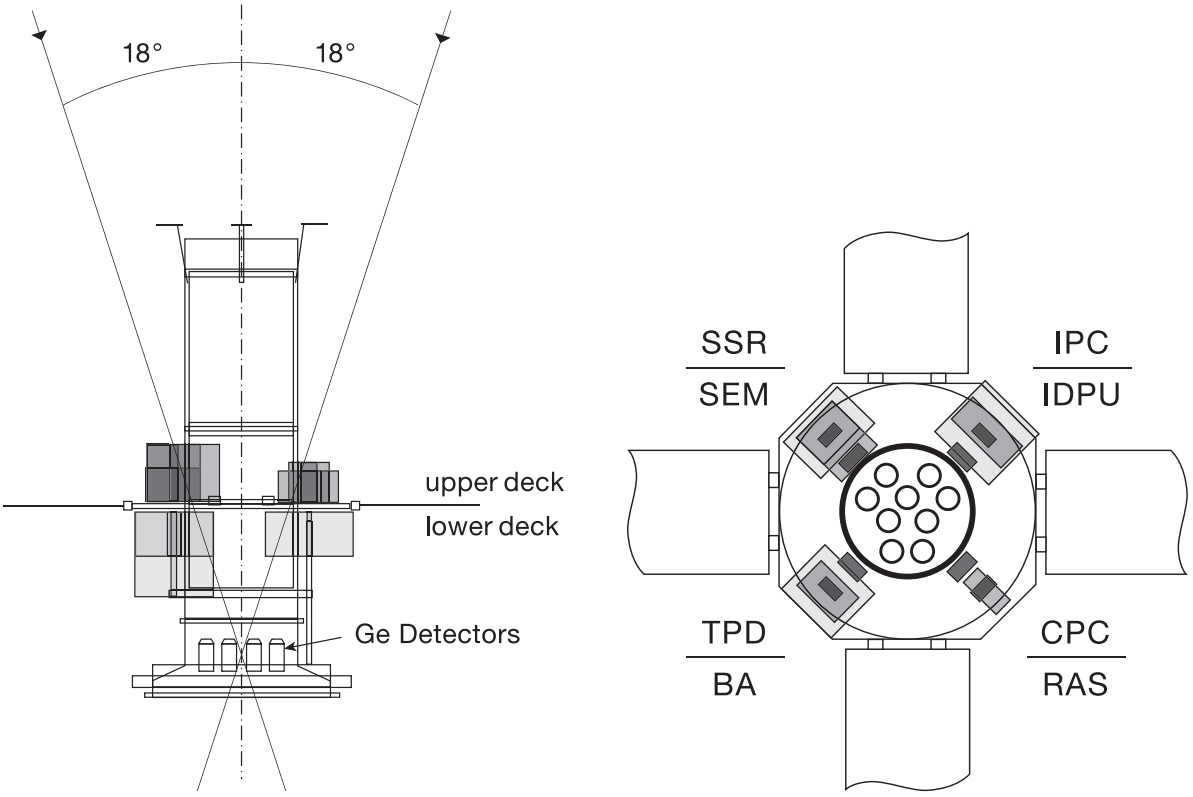


Fig. 2.— Schematic view of the locations of the support modules. On the solar direction of the equipment deck (i.e. above) are mounted: Solid State Recorder (SSR), Transponder (TPD), Cryocooler Power Converter (CPC), and Instrument Power Converter (IPC). The support modules mounted below the equipment deck are: Spacecraft Electronics Module (SEM), Battery (BA), photomultiplier Roll Angle System (RAS), and Instrument Data Processing Unit (IDPU). Photons from GRB021206 came in at an angle of 18° with respect to the Sun's direction.

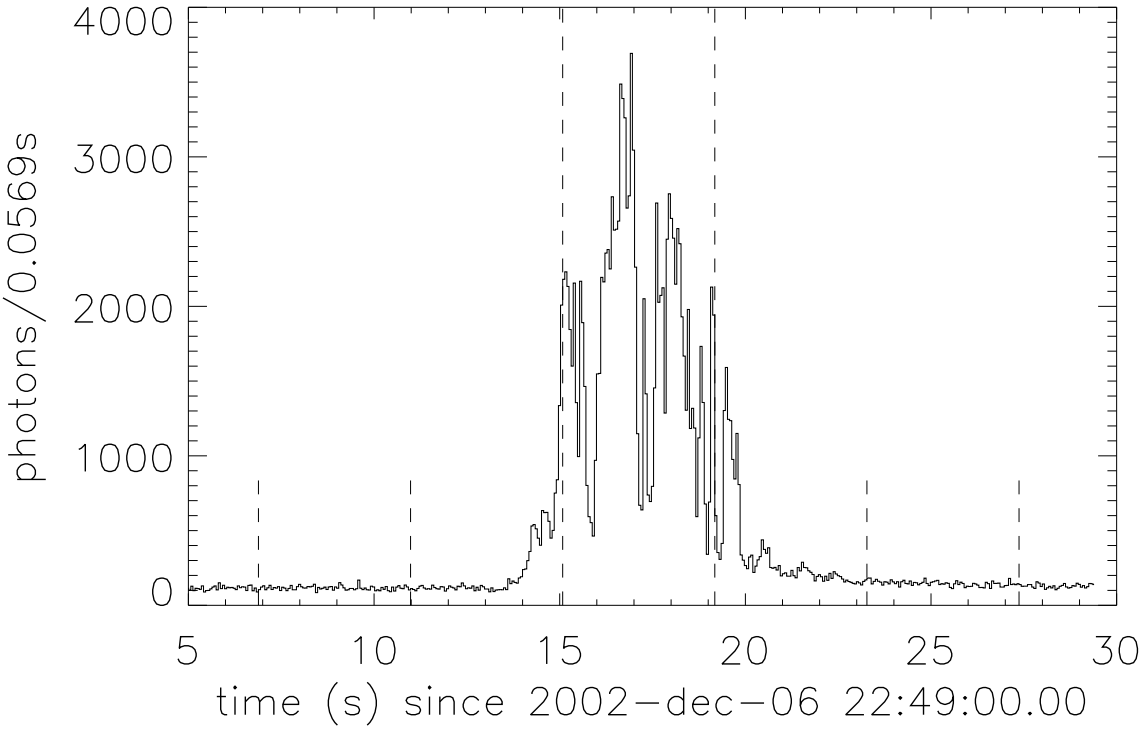


Fig. 3.— Light curve of GRB021206 in the 25 – 2000 keV band. Marked are the time intervals used for polarization analysis (Eq. (2)) and for background determination.

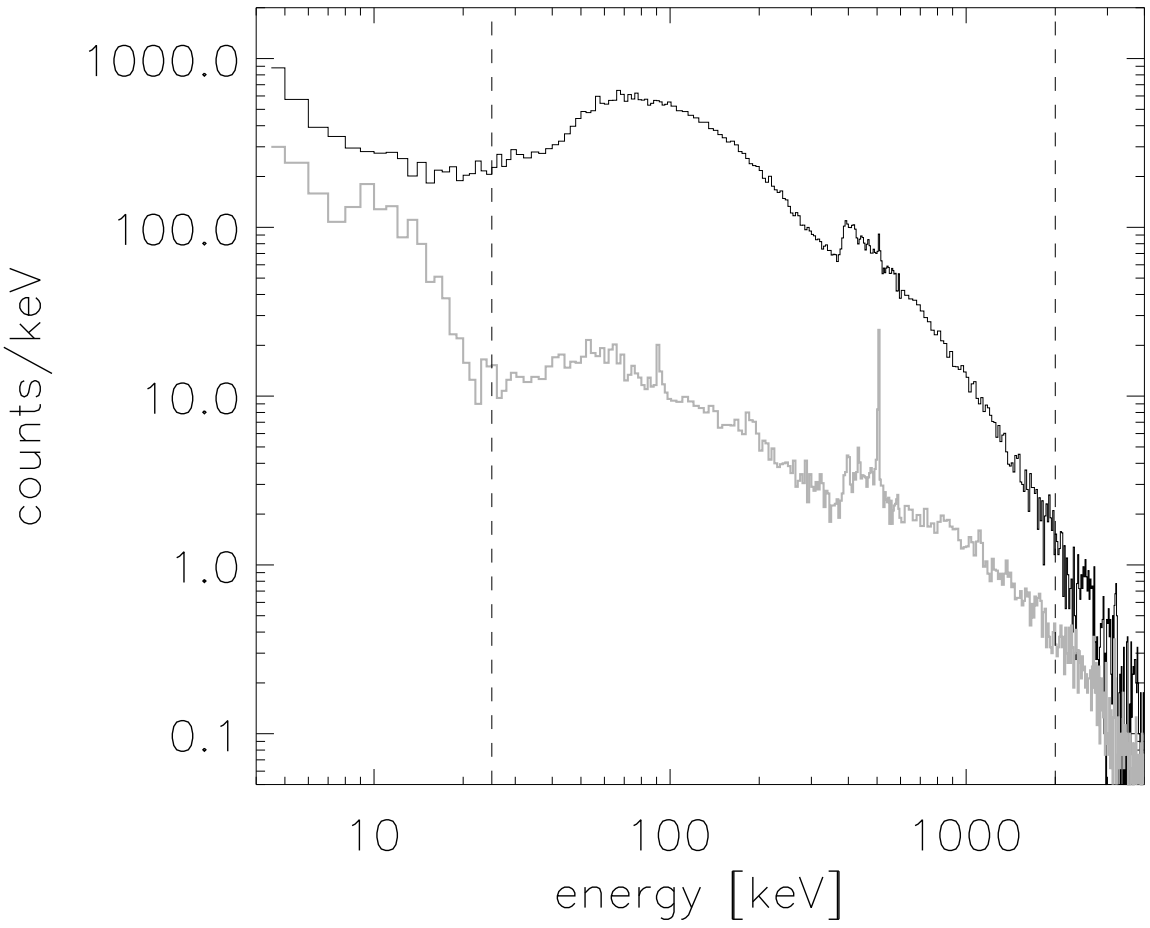


Fig. 4.— Energy distribution in the time interval marked in Fig. 3. Black: raw spectrum of all events. Gray: background spectrum, estimated from a time interval before and after the GRB.

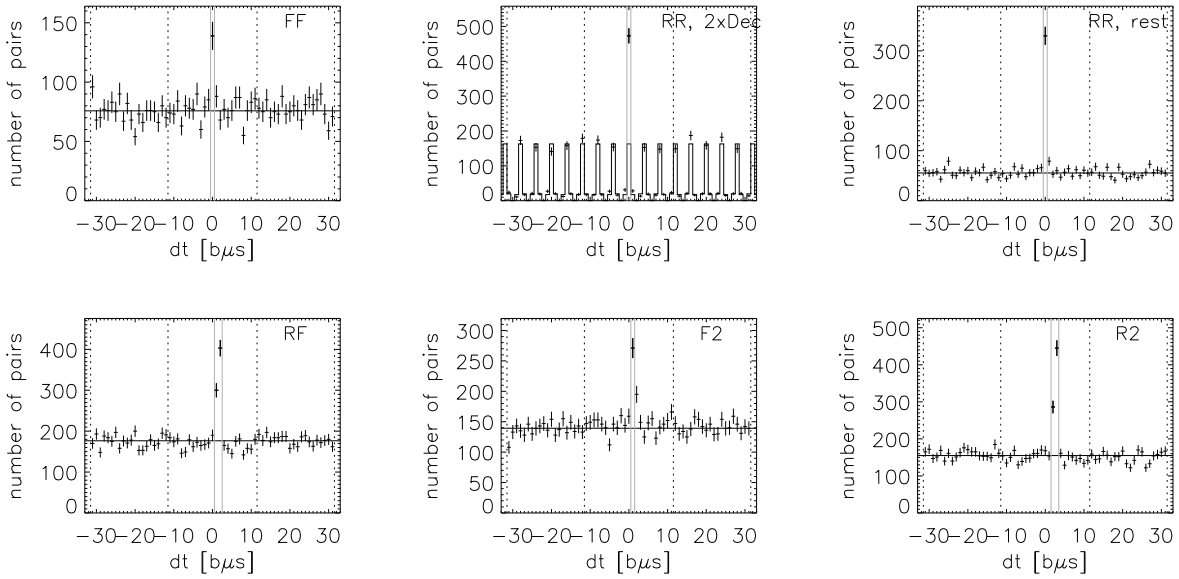


Fig. 5.— Distribution of time differences $dt$ between any two photons in the event list (belonging to the time interval (2), fulfilling the energy cut (5), the kinematical cut (7), and the close pairs cut), plotted for different combinations of electronics involved. The values in both intervals marked by the vertical dotted lines were used to interpolate the distribution around $dt = 0$. The interpolation is illustrated by a solid line. Real coincidences appear only in a few bins with $0\mathrm{b}\mu\mathrm{s} \leq dt \leq 3\mathrm{b}\mu\mathrm{s}$. (Multiple coincidences are included in these plots.)

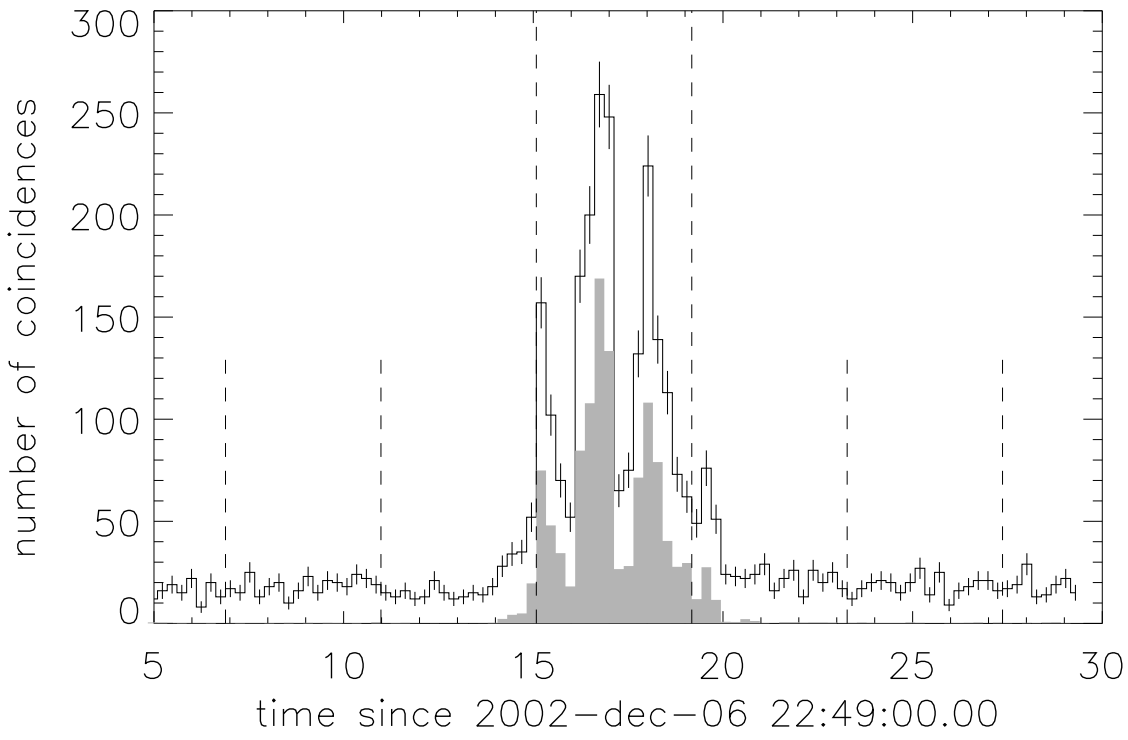


Fig. 6.— Light curve of coincidences. Black line histogram: total number of coincidences per bin ($N_{tot}$). Gray filled histogram: accidental coincidences ($N_{acc}$). The time bin width is $T_{rot}/16$. The long vertical lines indicate the time interval chosen for the polarization analysis. The short vertical lines indicate the intervals used to estimate the background contribution ($N_{BG}$).

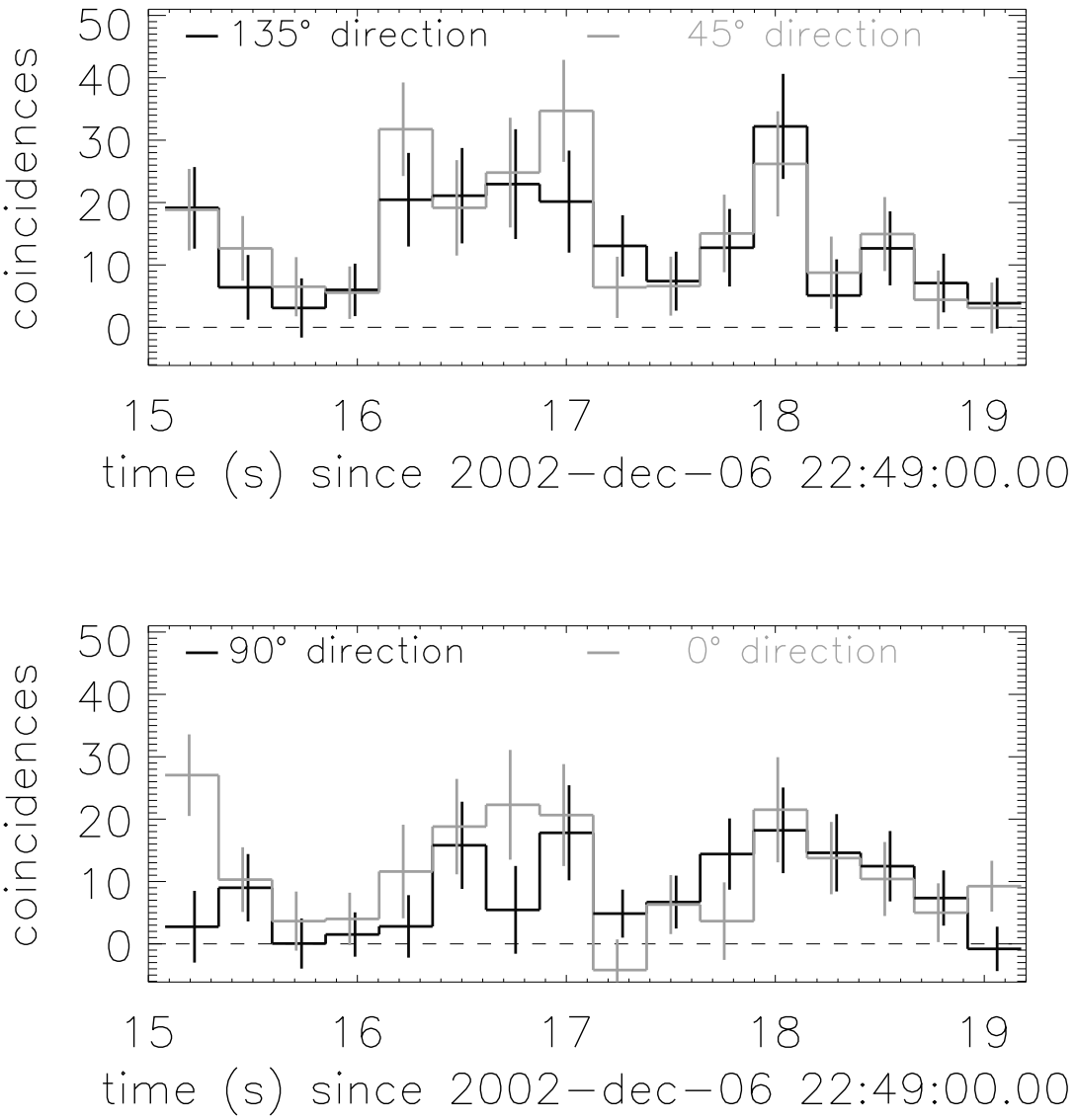


Fig. 7.— Time distribution of Compton scattering candidates, for the 4 different scattering directions given by the layout of the RHESSI detectors (see Fig. 1). The time bin width is 1/16th of a full rotation, as in Fig. 6. Two orthogonal directions are shown in the same plot. If one curve of a plot – in case of a polarized burst – showed a relative maximum, the other curve would have a relative maximum 4 bins later and earlier.

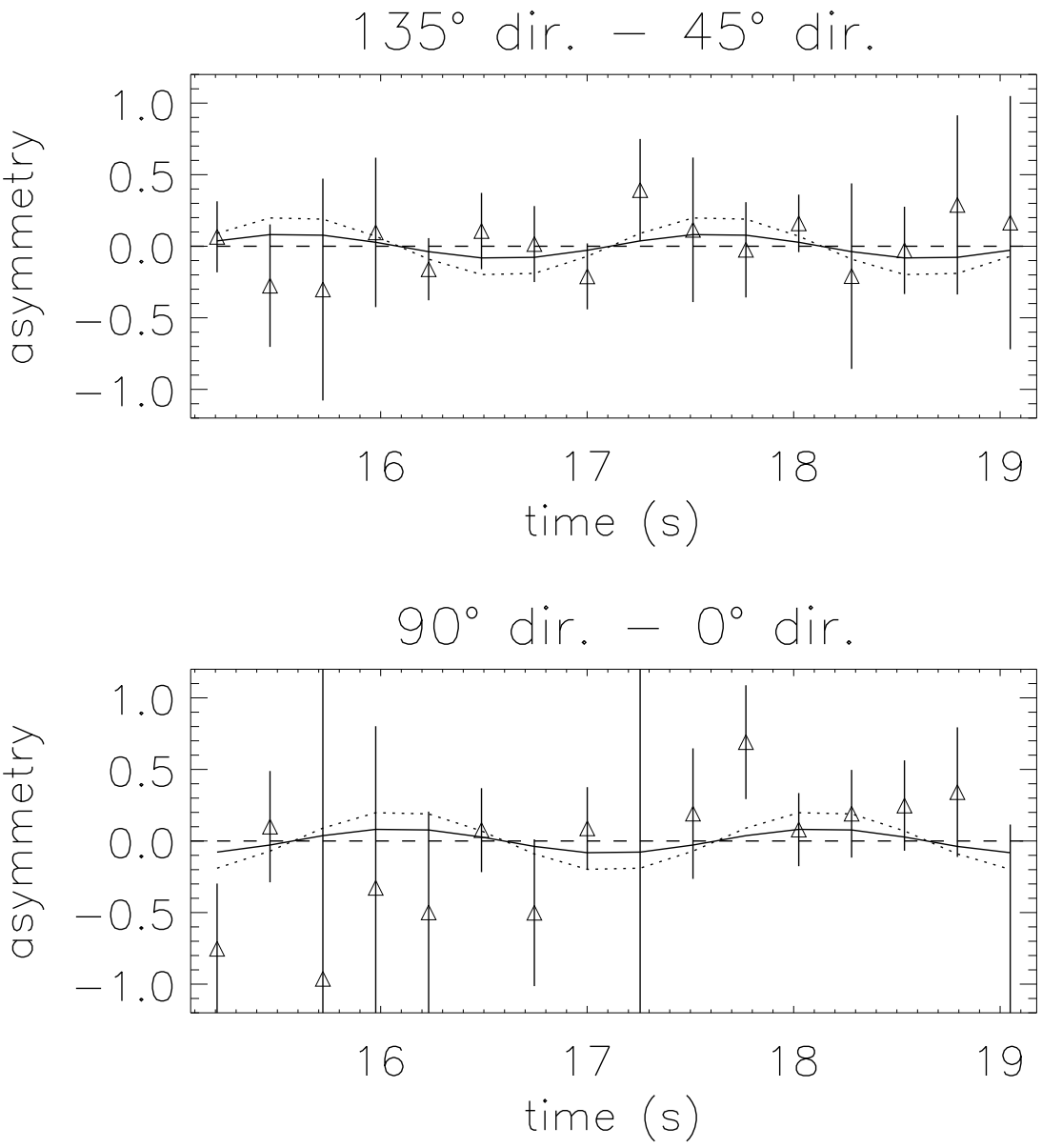


Fig. 8.— Asymmetries of the curves shown in Fig. 7, as defined in Eq. (12). The two plots are fitted simultaneously. The black line is the best fit of a sine-function, see Eq. (14), where the amplitude and phase are treated as free parameters. The dotted line has an amplitude as a fully polarized GRB would make (see Eq. (19)). Obviously, no significant statement about the polarization degree of GRB021206 can be made.

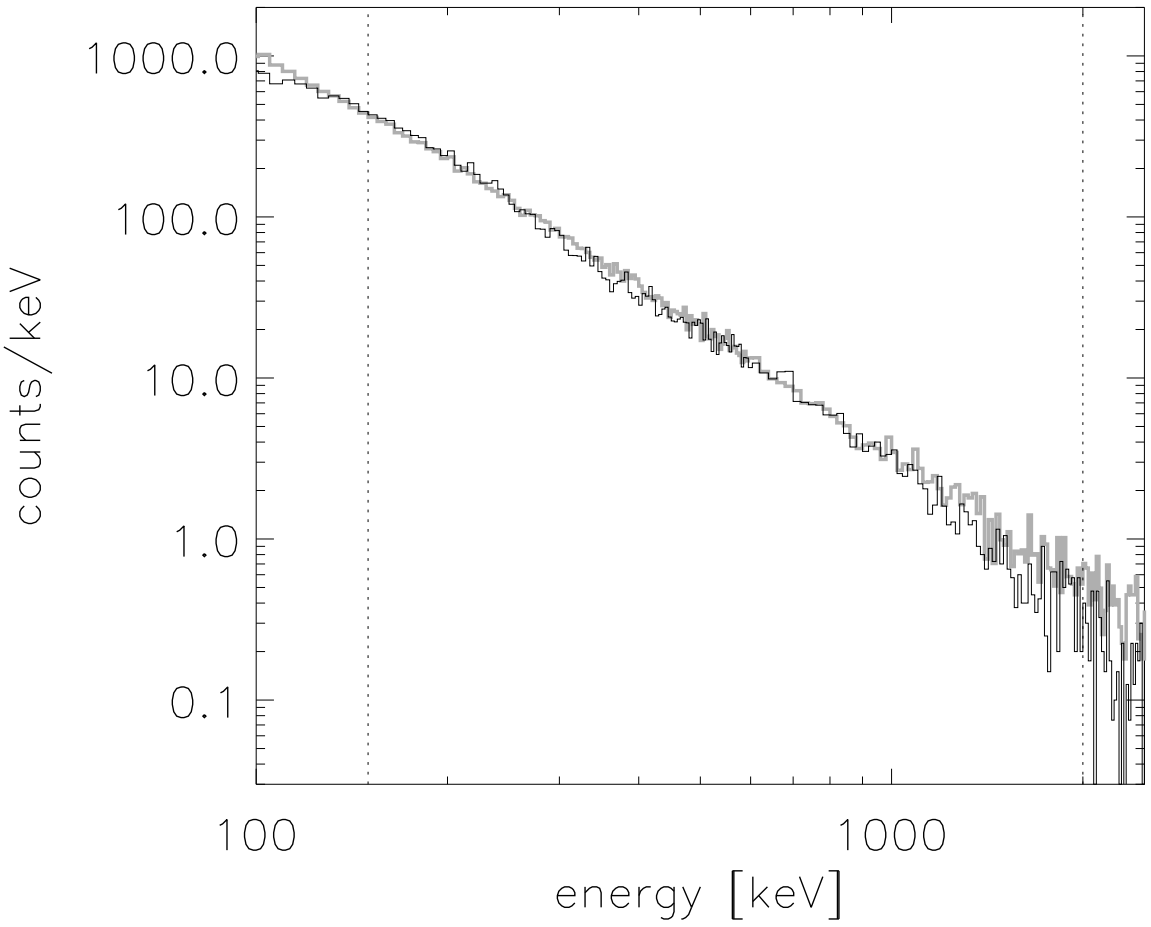


Fig. 9.— Observed energy spectrum of GRB021206 (black), summed over all detectors and segments (except detector 2). The background was subtracted, and the spectrum is corrected for decimation (unlike Fig. 4). The gray histogram is the result of a simulation with $dN/dE \propto E^{-2.6}$.

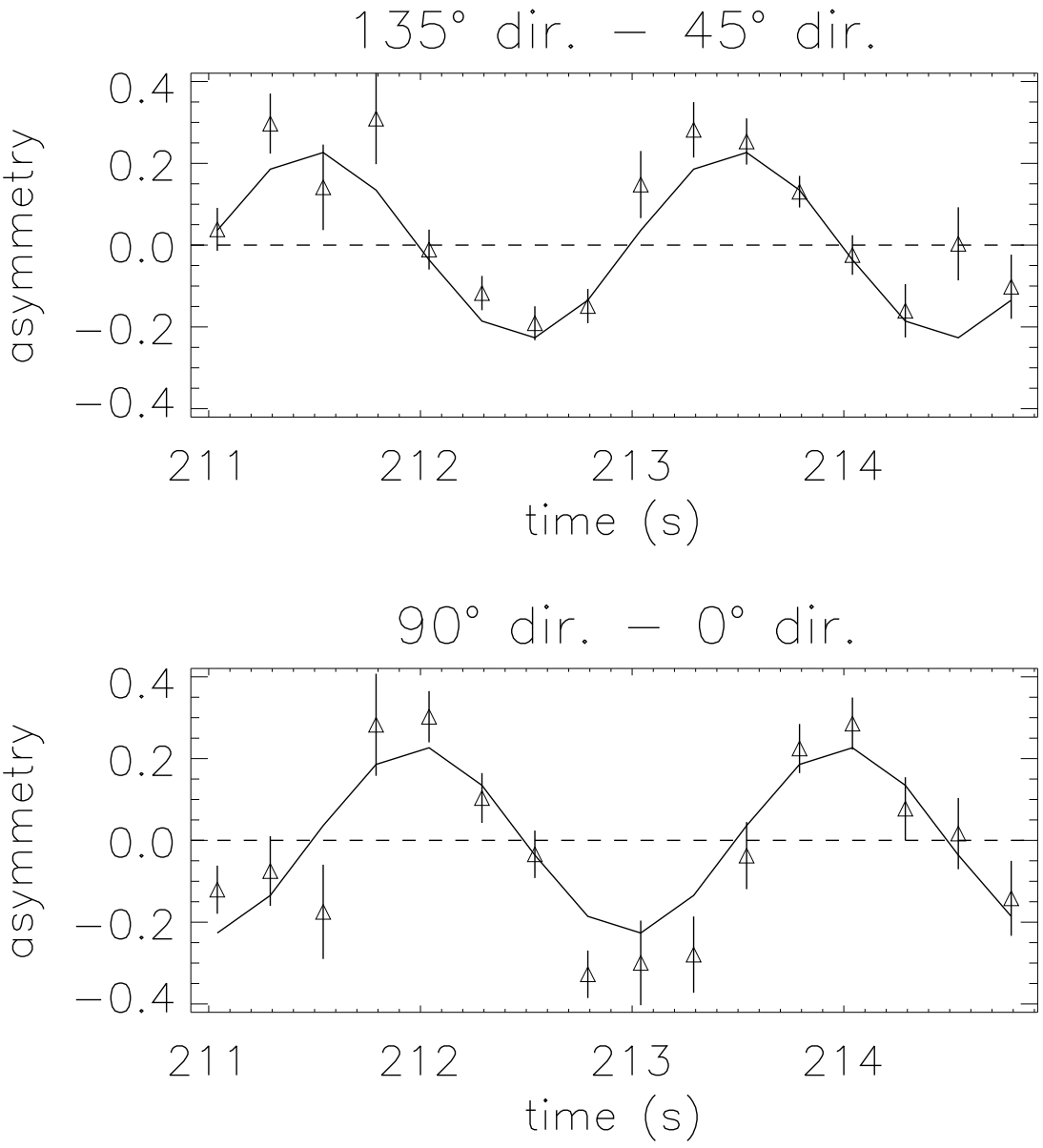


Fig. 10.— Similar to Fig. 8, but for simulated data. The simulation includes decimation and the light curve variability. The time offset is arbitrary, and $T_{rot,sim} = 4.0\,\mathrm{s}$. The fitted amplitude is given in Eq. (19).

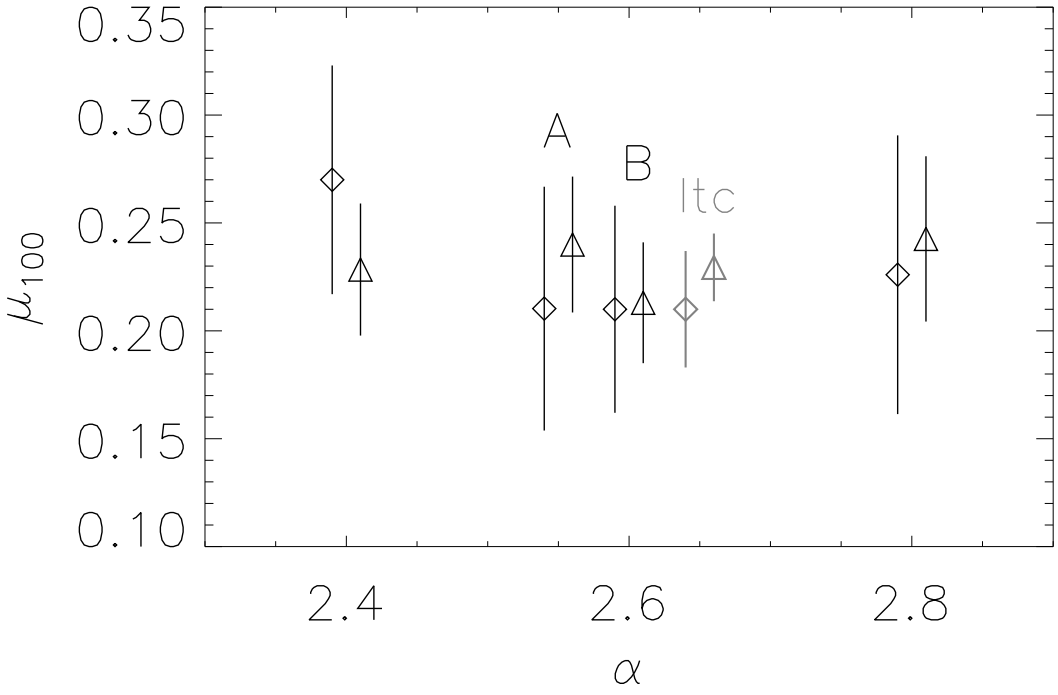


Fig. 11.— Modulation amplitude $\mu_{100}$ of a 100% polarized GRB for different power law indices $\alpha$. Diamonds: the simulated data were decimated. Triangles: simulated data without decimation. At $\alpha = 2.6$, we made two simulations with uniform time distribution ('A' and 'B') and one taking into account the light curve variability ('ltc', see also Fig. 10 and Eq. (19)).

Table 1. Counts per detector segment

| detector | front | rear | total |
|---|---|---|---|
| 1 | 6971 | 8147 | 15118 |
| 2 | 24788 | 0 | 24788 |
| 3 | 6274 | 7387 | 13661 |
| 4 | 5782 | 8280 | 14062 |
| 5 | 6676 | 6523 | 13199 |
| 6 | 4306 | 7482 | 11788 |
| 7 | 5293 | 7500 | 12793 |
| 8 | 6106 | 7850 | 13956 |
| 9 | 3651 | 7797 | 11448 |
| total | 69847 | 60966 | 130813 |

Note. — Number of counts in each detector, time and energy interval as indicated in Fig. 3 and Fig. 4.

Table 2. Number of coincidences, efficiency of cuts

| applied cuts | ref. | $N_{tot}$ | $N_{acc}$ | $N_{BG}$ | $N_C$ |
|---|---|---|---|---|---|
| time interval | Eq. (2) | | | | |
| and energy cut | Eq. (5) | | | | |
| and $\lvert dt\rvert \leq 3\,\mathrm{b}\mu\mathrm{s}$ | | 16542 | 13468.8 | 1432.0 | $1641 \pm 141$ |
| $dt$-cut | Eq. (8) | 6030 | 3322.6 | 1172.9 | $1535 \pm 83$ |
| close pairs cut | §3.2 | 4135 | 1868.6 | 790.5 | $1476 \pm 69$ |
| kinematical cut | Eq. (7) | 2647 | 1093.7 | 512.6 | $1041 \pm 55$ |
| no-multiples | §4.1 | 2141 | 1081.0 | 290.3 | $770 \pm 49$ |

Note. — The total number of coincidences ($N_{tot}$), the number of accidental coincidences ($N_{acc}$), and the number of background coincidences ($N_{BG}$) are listed after each additional data cut was applied. The corresponding statistical errors are: $\sqrt{N_{tot}}$, $\sqrt{N_{acc}/10}$, $\approx \sqrt{N_{BG}/2}$. The number of Compton scattering candidates ($N_C$) is obtained according to Eq. (10).

Table 3. Number of coincidences, comparison with previous work

| | $N_{tot}$ | $N_{acc}$ | $N_{BG}$ | $N_C$ |
|---|---|---|---|---|
| CB | 14916 | $4488 \pm 70$ | $588 \pm 24$ | $9840 \pm 96$[a] |
| RF | 8230 | $6640 \pm 80$ | $760 \pm 110$ | $830 \pm 150$ |
| present work | 2141 | $1081 \pm 10$ | $290 \pm 12$ | $770 \pm 49$ |
| "our CB" | 15810 | $13786 \pm 37$ | $848 \pm 21$ | $1176 \pm 138$ |
| "our RF" | 7788 | $6329 \pm 25$ | $648 \pm 18$ | $811 \pm 93$ |

[a]Error as quoted by CB. From error propagation, this error is expected to be $> \sqrt{N_{tot}}$, i.e. $> 122$ .

Note. — The total number of coincidences ($N_{tot}$), number of accidental coincidences ($N_{acc}$), number of background coincidences ($N_{CB}$) and number of Compton scattering candidates ($N_C$) are compared with previous works. The lines "our CB/RF"report on our attempts to reproduce CB's and RF's numbers by using cuts similar to theirs. See text for details of the cuts used.